Experimental study on the effects of spray-wall interaction on partially premixed combustion (PPC) and engine emissions

energy&fuels

Combustion

Experimental study on the effects of spray-wall interaction on partially premixed combustion (PPC) and engine emissions

Qinglong Tang, Yanzhao An, Vallinayagam Raman, Hao Shi, Jaeheon Sim, Junseok Chang, Gaetano Magnotti, and Bengt Johansson

Energy Fuels, **Just Accepted Manuscript** • DOI: 10.1021/acs.energyfuels.9b00602 • Publication Date (Web): 01 May 2019

ACS Publications

is published by the American Chemical Society. 1155 Sixteenth Street N.W., Washington, DC 20036

Experimental study on the effects of spray-wall interaction on partially premixed combustion (PPC) and engine emissions

Qinglong Tang[a], Yanzhao An[a,*], Vallinayagam Raman[b], Hao Shi[a], Jaeheon Sim[b], Junseok Chang[b], Gaetano Magnotti[a], Bengt Johansson[a]

[a]Clean Combustion Research Center (CCRC), King Abdullah University of Science and Technology (KAUST), Thuwal, Saudi Arabia

[b]Fuel Technology Division, R&DC, Saudi Aramco, Dhahran 31311, Saudi Arabia

Abstract

We investigated the detailed spray-wall interaction in partially premixed combustion (PPC) in an optical engine with a wide-angle injector at low engine load. The fuel-trapping effect of the piston top-land crevice was visualized by fuel-tracer planar laser-induced fluorescence (PLIF) for the first time. In agreement with the fuel distribution shown by PLIF, the combustion region first moves into the squish region and then tends to move back to the piston bowl when advancing the injection timings. Results indicate that a considerable portion of the fuel is trapped in the piston top-land crevice for the cases with injection timings at -30° (SOI-30 case) and -40° (SOI-40 case) CA aTDC. The SOI-40 case with earlier injection timing presents a backflow process of the trapped fuel from the piston top land crevice to the squish region. However, there is not enough time for the fuel vapor to flow back before the start of combustion for the SOI-30 case, resulting in a relatively lower fuel-air equivalence ratio in the squish region and thus higher CO emission than the SOI-40 case. This study provides insights into the fuel distribution characteristics in piston crevice and the potential effects on the engine emissions under PPC condition.

Keywords: PPC; Spray-wall interaction; PLIF; Fuel-trapping effect; Piston top-land crevice

1. Introduction

Conventional diesel compression-ignition engine (CI) has high efficiency and excellent durability but it suffers from increased NO_x and soot emissions due to the feature of mixing-controlled combustion. Homogeneous charge compression ignition (HCCI) can achieve lower NO_x and soot emissions through premixed fuel-air charge and low-temperature combustion. However, the combustion phasing of HCCI, dominated by the chemical kinetics, is difficult to control. Besides, the excessive pressure rise rate (PRR) at medium-high engine load limits the upper operating range of HCCI [1-3]. As an intermediate process between HCCI and CI, partially premixed combustion (PPC) adopts earlier fuel injection timings than CI. Therefore, the fuel has more time for pre-mixing before ignition, which favors the low-temperature combustion. Meanwhile, a certain level of fuel stratification is maintained so that the combustion phasing can be well controlled with a restrained peak PRR [4].

The decoupling of the fuel injection and the ignition process, i.e. a positive ignition dwell, is crucial for PPC. It is a sign of sufficient fuel-air mixing and normally could lead to low-temperature combustion. Using fuels like diesel and n-heptane, PPC can be easily implemented with an early start-of-injection (SOI) timing and a moderate exhaust gas recirculation (EGR) at low-medium engine load [5, 6]. However, at high engine load, it requires too much EGR to get a positive ignition dwell. This results in lower combustion efficiency and fuel penalty with a sharp increase in the unburned hydrocarbon (UHC) and carbon monoxide (CO) emissions [7, 8]. On the other hand, for fuels like gasoline and iso-octane, a positive ignition dwell can be realized at the medium-high engine load with a moderate EGR rate [9, 10]. These fuels have a higher resistance to auto-ignition and prolong the ignition delay to enhance the fuel-air mixing process. Engine experiments on gasoline PPC showed that an indicated engine efficiency higher than 50% could be achieved [11]. However, a major challenge to PPC using gasoline-like fuels comes from the combustion stability at low engine load when the overall fuel-air charge is overly lean [12, 13]. The best fuel for PPC operation seems to be in between that of diesel and gasoline. Hildingsson et al. [14] investigated the PPC engine performance and emissions using gasoline fuels with different research octane number (RON). They observed that the optimum RON range was between 75 and 85 in the conditions studied. Recently, PPC operated with low-octane fuel like dieseline (a mixture of the diesel and gasoline) and naphtha at low load condition gained more attention due to the improvement of the combustion stability and engine efficiency [15, 16].

PPC adopts early fuel injection strategy that produces longer fuel spray penetration length due to the relatively lower in-cylinder pressure and temperature at the time of injection [17]. This could result in an interaction between fuel sprays and walls, especially when using a traditional diesel injector with a wide spray angle [18, 19]. Herein, the “walls” refers to the surfaces of the piston top, cylinder wall and piston

top-land. Many studies considered the spray-wall interaction to be closely related to the high emissions of UHC and CO in PPC mode at low load [20, 21]. Peterson et al. [22] explored the fuel distribution in PPC mode at a low engine load of 3 bar gross indicated mean effective pressure (IMEP) using quantitative fuel-tracer planar laser-induced fluorescence (PLIF) imaging in an optical engine. The fuel injection timing was at -23° crank angle after top dead center (CA aTDC) with a global fuel-air equivalence ratio of 0.3. They found that a portion of the fuel was directly injected into the squish region forming a local overly rich mixture with equivalence ratio from 1.0 to 1.4. Most of the fuel was directed into the lower part of the piston bowl prior to ignition. It forms an overly lean mixture with equivalence ratio from 0.1 to 0.5 in the middle-upper part of the piston bowl near the injector nozzle. They predicted that most of the UHC and CO emissions originated from the overly lean mixture ($0.1< \phi <0.5$) in the piston bowl and squish region, and a small part of CO derived from the overly rich mixture ($1.0 < \phi <1.4$) in the squish region. Wang et al. [23] studied the spray-wall interaction under different fuel injection timings by qualitative fuel-tracer PLIF imaging. They believed that the fuel-trapping effect in the squish region was responsible for the increased UHC and CO emissions when using early fuel injection timings.

In the above-reviewed literature, the piston top-land crevice was not visualized due to the limited view field in the optical engine setups. Actually, the fuel trapped in the piston top-land crevice under early injection condition has long been suspected to be an important source of UHC and CO emissions under PPC mode [24-26]. However, few studies have been concentrated on the spray-wall interaction involved with the piston top-land crevice. The understanding of the distribution characteristics of the fuel trapped in the piston top-land crevice is quite limited. Besides, the effects of different fuel injection timings on the in-cylinder fuel distribution situations and the following combustion process at PPC mode still need further investigation.

Therefore, in the present study, the detailed spray-wall interaction under different fuel injection timings was studied in an optical engine under PPC mode at low engine load. The behavior of the fuel trapped in the piston top-land crevice was visualized by fuel-tracer PLIF imaging for the first time. A low-octane fuel of PRF77 (a mixture of 77% iso-octane and 23% n-heptane by volume) was directly injected at different timings. Toluene of 1% by volume served as the tracer for the fuel vapor under non-combusting condition. A high-speed camera captured the natural flame luminosity (NFL) images from 50 consecutive fired cycles. A flame probability distribution index was calculated and linked to the fuel distribution obtained by the PLIF imaging. The effects of fuel injection timings on the engine-out UHC and CO emissions were analyzed combining the fuel distribution information. This work aims to gain insight into the in-cylinder spray-wall interaction and combustion characteristics of PPC at low engine load. It also contributes valuable experimental data for the validation of the three-dimensional simulation

for the spray-wall interaction under PPC condition.

2. Experimental setup and optical diagnostic techniques

2.1 Optical engine and operating conditions

A light-duty, single-cylinder AVL optical engine was employed in this study. The main engine specifications are listed in Tab. 1. The piston of the engine has a quartz piston crown and an extended piston sleeve that allows for the optical access. The piston crown has a ω-shape bowl with a curved bottom surface, as shown in Fig. 1a. It enables the entrance of the vertical laser sheet into the combustion chamber and made the whole squish region visible near the top dead center (TDC). The diameter of the combustion chamber is 50.8 mm. A quartz liner with an outer diameter of 135 mm and a height of 29 mm is aligned into the upper part of the cylinder wall by a hydraulic system. The laser sheet passes through the quartz liner and the in-cylinder process is visible from the side view. The engine is equipped with a Bosch common-rail injector. The injector nozzle is located in the center of the cylinder and had eight orifices with a spray angle of 162°. The eight orifices are evenly spaced with a diameter of 0.18 mm.

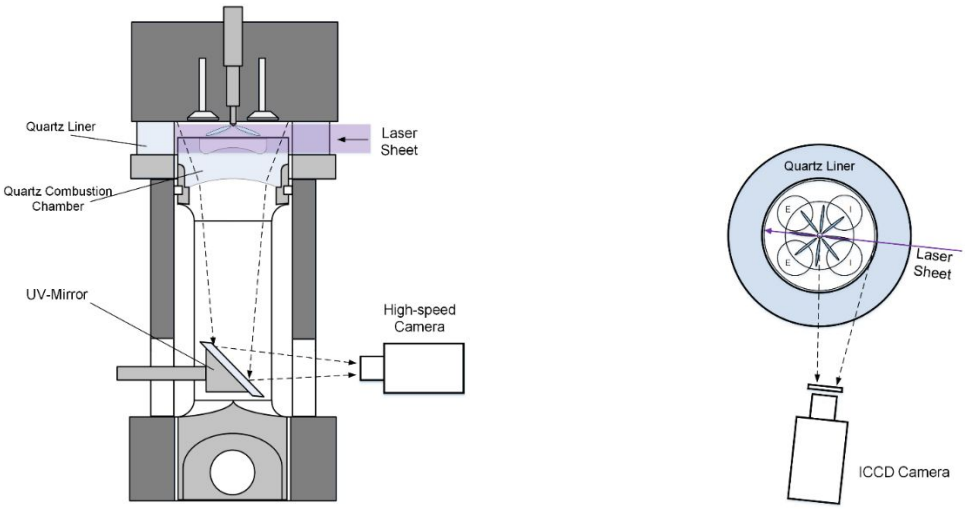

(a) Side view (b) Top view

Fig. 1. Schematic of the optical engine and the laser location relative to the fuel sprays and combustion chamber. Note that the natural flame luminosity imaging and PLIF imaging were carried out separately and the laser was turned off when using the high-speed camera.

The fuel injection timing, pressure and duration were controlled through the AVL FI2RE software. A heater was installed in the intake manifold to preheat the supplied air to support the auto-ignition of the low-octane fuel. A pressure transducer measured the in-cylinder pressure during the engine combustion process with a resolution of 0.2° CA. The pressure data was processed to get the averaged heat release rate. The NO_x, CO and UHC emissions in the exhaust pipe were measured by the AVL AM i60 test bench. The engine was run at a speed of 1200 revolutions per minute (rpm) without EGR. The intake pressure and temperature were 1.5 bar and 413 K, respectively, producing a motored TDC pressure of 35 bar and

TDC temperature of 872 K. The engine coolant and lubrication temperature were kept at 333 K. The injected PRF77 mass for each cycle was 14 mg and the global equivalence ratio was 0.28. The fuel injection duration was about 8° CA for all cases with the start of injection (SOI) timings from -20° to -60° CA aTDC. The cases with SOI timings at -20°, -30°, -40° and -60° CA aTDC were denoted as SOI-20, SOI-30, SOI-40 and SOI-60, respectively.

Tab. 1. Optical engine specifications.

Bore	85 mm
Stroke	90 mm
Displacement	0.51 L
Connecting rod length	138 mm
Compression ratio	9.5
Combustion chamber shape	ω
Intake valve number	2
Intake valve open at	30° CA bTDC
Intake valve closed at	45° CA aBDC
Exhaust valve number	2
Exhaust valve open at	50° CA bBDC
Exhaust valve closed at	25° CA aTDC

Tab. 2. Engine operating conditions

Engine speed	1200 rpm
Intake pressure	1.5 bar
Intake temperature	413 K
Coolant temperature	333 K
Lubricant temperature	333 K
Fuel Injection pressure	600 bar
Fuel	PRF77
Fuel mass	14 mg/cycle
Start of injection (SOI)	-20°~-60° CA aTDC
Global equivalence ratio	0.28

Air was supplied in the intake stroke for the combusting engine cycles during the high-speed NFL experiment. While the engine was fired for 150 consecutive cycles, the cylinder pressure and NFL images of the last fired 50 cycles were used for post-processing. In the fuel-tracer PLIF experiment, the intake air was replaced by pure nitrogen to eliminate the oxygen quenching effect on toluene PLIF signal. Tab. 2 summarizes the main engine operating conditions.

2.2 Fuel-tracer PLIF imaging

The fuel-tracer PLIF imaging was carried out under non-combusting condition by supplying the intake with pure nitrogen. A10 Hz crank signal was produced by the engine to trigger the Nd:YAG laser (Q-smart 850, Quantel) through a pulse delay generator (DG535, Stanford Research). The fourth harmonic (266 nm, 60 mJ/pulse) was chosen for the toluene tracer excitation. The laser beam was formed into a vertical laser sheet less than 1 mm thick and 20 mm high by the LaVision sheet and collimator optics. The

laser sheet was located just below the bottom of the cylinder head. It passed through the center of the cylinder head, intersecting two of the fuel sprays, as shown in Fig. 1b.

A crank signal from the engine triggered the ICCD camera (PI-MAX3, Princeton Instruments) to capture the toluene fluorescence signal after the start of fuel injection. The ICCD camera, equipped with a 105 mm, f/4.5 UV-lens, was placed on the side of the quartz liner and perpendicular to the laser sheet. A band-pass filter (FF01-292/27, Semrock) with a transmission range of 278.5-305.5 nm was coupled to the lens to collect the toluene PLIF signal. The gate-width and gain level were set to 100 ns and 90, respectively. The pulse delay generator synchronized the timing sequence of the signals for the laser, engine and camera.

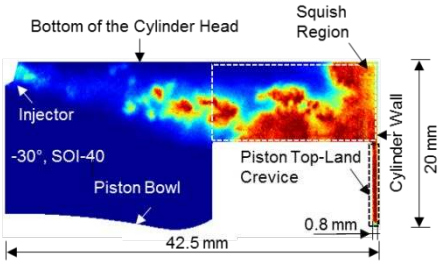

(a) Single-shot fuel-tracer PLIF image in false color

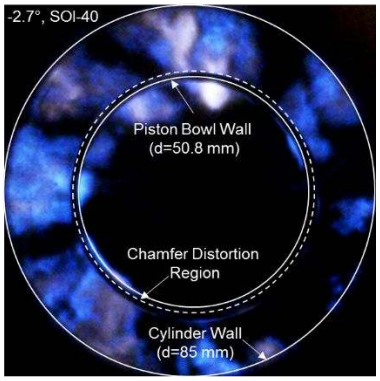

(b) Single-shot NFL image in true color

Fig. 2. View field of the ICCD camera for the fuel-trace PLIF from the side of the piston at -30° CA ATDC for the SOI-40 case (a) and the high-speed camera for the natural flame luminosity (NFL) imaging from the bottom of the piston at -2.7° CA ATDC for the SOI-40 case (b). The squish region and piston top-land crevice are marked by two dashed rectangles in Fig. 2a.

Thirty PLIF images were acquired from 30 consecutive engine cycles at each specified crank angle. The image distortion caused by the optical liner and piston bowl was corrected. More detail about the image distortion correction is in the Appendix. The correlation coefficient between each single-shot image and the averaged image was calculated. The one with the maximum correlation coefficient was chosen as a representative.

The view field of the ICCD camera is illustrated in Fig. 2a by a single-shot PLIF image of the fuel spray on the right-hand side shown in Fig. 1b. The PLIF image presents a clear view of the interaction among the fuel spray, piston bowl and squish region. The fuel distribution in the piston top-land crevice

(about 0.8 mm in width) can also be clearly visualized. This provides important information about the fuel trapped in the top-land crevice. Note that the height of the top-land crevice, i.e., the distance between the piston top and the first piston ring, was about 40 mm but only the region swept by the laser sheet (20 mm high) was visualized.

2.3 High-speed natural flame luminosity (NFL) imaging

When the high-speed NFL images were measured, the laser and ICCD camera were shut down and the intake gas was changed to air. A high-speed CMOS camera (Photron Fastcam SA4) was used to record the NFL during the combustion from the bottom view of the piston through a UV-mirror. One example of the NFL image is shown in Fig. 2b. A 50 mm, f/1.4 lens was coupled to the high-speed camera. The frame rate and exposure time of the camera were set to 10000 frames per second and 100 μs, respectively. Thus, the temporal resolution of the acquired images was 0.72° CA at the engine speed of 1200 rpm.

During the experiment, the NFL image sequences for 50 consecutive fired engine cycles were recorded simultaneously with the cylinder pressure so that the gross IMEP can be correlated with the NFL intensity. In order to minimize the interference from soot radiation, the blue channel of the RGB image was extracted to represent the chemiluminescence in the early stage of the combustion. The distortion caused by the curved surfaces of the piston crown window was corrected as shown in the Appendix.

A flame probability distribution index (PDI) was calculated to describe the flame distribution in the cylinder. PDI describes the probability of flame occurrence at any specified pixel (*x, y*). To do this, we need to know how often the flame appears at the pixel (*x, y*) in each image. So a binarization process was carried out to answer yes or no at pixel (*x, y*) for each image. A threshold of 10% of the maximum signal intensity, $I_{threshold}$, for each image was employed. If the signal intensity at pixel (*x, y*) is lower than $I_{threshold}$, the intensity of the binarized image at pixel (*x, y*), $i_{(x,\ y)}$, is assigned to 0, indicating no flame in this location. Otherwise, it is assigned to 1. Finally, the PDI at location (*x, y*), $\mathrm{PDI}_{(x,y)}$, was obtained by statistics on the 50 binarized images using the following equation. PDI of 0 means there is no flames in the specified region, while PDI of 1 means flames always appear in location (*x, y*). This procedure was applied to every pixel of the image to get the PDI distribution in the whole cylinder.

$$PDI_{(x,\ y)} = \left(\sum_{1}^{50} i_{(x,y)}\right)/50$$

3. Results and discussions

3.1. Analysis of engine-out emissions, rate of heat release and natural flame luminosity

The engine-out emissions of CO, UHC, and NO_x under different SOI timings from -10° CA aTDC to -120° CA aTDC are shown in Fig. 3. NO_x emission reduces gradually to near zero while UHC and CO

increase to a plateau with advanced SOI timings from -10° to -60° CA aTDC. There is no big change in emissions at SOI earlier than -60° CA aTDC. Note that the CO emission of the SOI-30 case is even higher than that of the SOI-40 case. This similar CO emission jump for the SOI-30 case was also observed when using fuels of PRF60 and naphtha under similar engine operating conditions in the author's previous works [16, 27]. This interesting phenomenon of the CO emission trend in PPC range could possibly be explained by the differences in spray-wall interaction situations. Thus, PPC cases with SOI from -20° to -60° CA aTDC are chosen for analysis of rate of heat release, NFL intensity and spray-wall interaction.

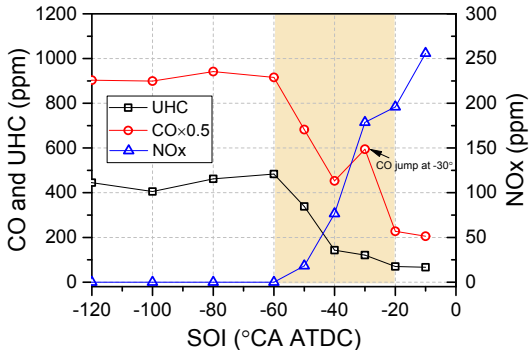

Fig. 3. Engine-out emissions of CO, UHC and NOx under the different start of injection (SOI) timings.

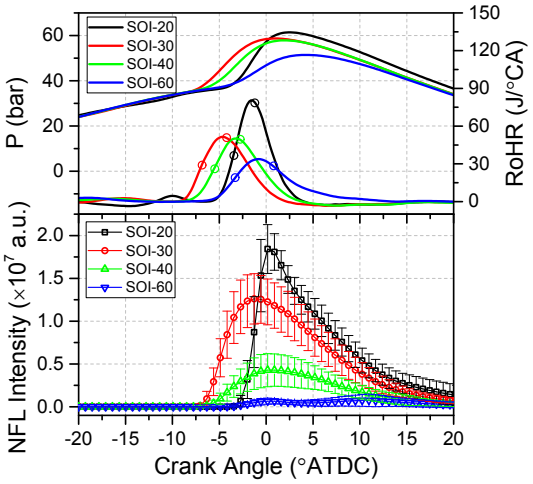

Fig. 4. Cylinder pressure (P), rates of heat release (RoHR) and NFL intensity averaged from 50 engine cycles of the PPC cases with different SOI timings. The two circles on the RoHR curves show the CA10 and CA50.

The peak cylinder pressures and rates of heat release become lower with the advancing of the SOI timing, as shown in Fig. 4. The CA10 (the crank angle when 10% of the total combustion heat is released) and CA50 for each case are marked by two circles on the rates of heat release curves. The combustion phasing, indicated by CA50, is first advanced and then retarded. The SOI-30 case presents the earliest combustion phasing compared to all other cases. Figure 4 also shows the NFL intensity with error bars averaged from 50 fired engine cycles for different SOI cases. The overall NFL intensity decreases with

the advancing of the SOI timings. Typical NFL images at CA50 for all four cases showing blue flames are presented in the upper panel of Fig. 5. The NFL intensity of the SOI-60 case is almost negligible compared to that of the SOI-20 case. The NFL signal is captured by the high-speed color camera in the spectral range of 350-700 nm and the chemiluminescence in the ultraviolet range like OH is not included. That's why the NFL intensity curves slightly lag behind the RoHR curves at the beginning of the combustion. Before the peak of the NFL intensity, most of the natural flame comes from the blue chemiluminescence derived from the band spectra of C_2, HCO, CH_2O and CH, and the continuum spectra of CO oxidation [28, 29]. After the peak of the NFL signal, soot radiation begins to emerge and gradually prevails. The heat release is negligible for all four cases at 5.2° CA and the NFL images, shown in the lower panel of Fig. 5, are dominated by soot radiation. This explains why the curves of the NFL intensity in Fig. 4 persist even after the end of the main heat release.

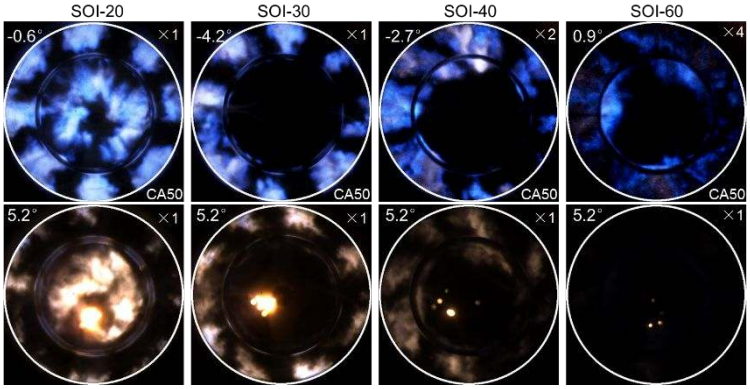

Fig. 5. Typical NFL images at CA50 and 5.2° CA aTDC for all cases. The NFL magnification factor is shown on the upper right of each image.

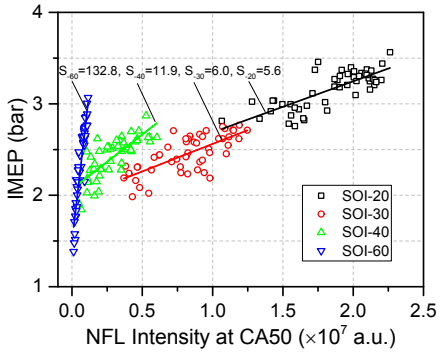

Fig. 6. Relationship between the gross IMEP and NFL intensity at CA50. The slops of each fitted curves are marked out.

Considering that the flame chemiluminescence during the main combustion is closely related to the heat release process, the images of the NFL at CA50 for all cases are chosen to evaluate the cycle-to-cycle variation in PPC mode. The plot of gross IMEP versus NFL intensity at CA50 in Fig. 6 essentially presents a linear relationship, i.e., the higher the NFL intensity, the larger the IMEP. The slopes of the linear fitting curves increase with the advancing of the SOI timings. For example, the slope of the SOI-20 case is about

5.6, while it is 132.8 for the SOI-60 case. This significant difference is because the overall NFL intensity variation for cases with different SOI timings is much larger than that of IMEP.

The evolution of flames during the combustion process for all four cases are presented in terms of flame PDI, as shown in Fig. 7. The higher the flame PDI index, the higher the probability of flame occurrence and vice versa. The images at CA10 show that the initial ignition kernels for all cases are located in the squish region closer to the cylinder wall. Flames emerge in the piston bowl later on for the SOI-20 case, and eight fuel jets can be clearly recognized by the separated flame regions at -1.3° CA. The combustion is mainly distributed in two regions at CA50 (-0.6° CA), the squish region and the piston bowl, which are separated by the bowl rim. The flames in the squish region gradually fade away after CA50 and the main flame region is confined in the piston bowl at 5.2° CA. As mentioned in Fig. 5, the NFL before CA50 mainly comes from the blue chemiluminescence and the NFL after 5.2° CA from soot radiation. The soot radiation due to the injector dribbling can be seen at 10.2° CA, as shown by the white arrows in Fig. 7. In the following 10° CA, the soot radiation in the piston bowl gradually decreases.

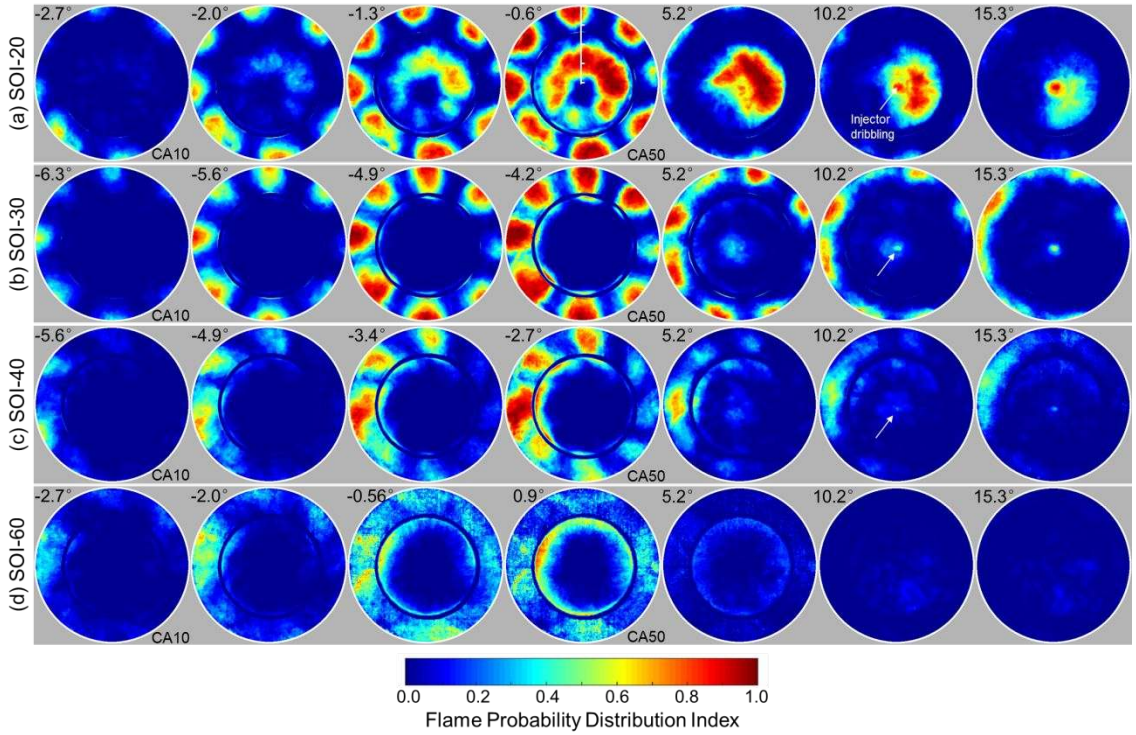

Fig. 7. The flame probability distribution index (PDI) of PPC cases with different SOI timings. The crank angle is marked on the upper left of each image. The first and fourth images of each sequence correspond to the CA10 and CA50, respectively. The white arrows mark the soot radiation of the injector dribbling.

In comparison to the SOI-20 case, a major difference in the flame PDI for SOI-30 case is that most of the flame is confined in the squish region and cannot be seen in the piston bowl before CA50. The soot radiation due to injector dribble emerges late after 5.2° CA but shows a lower flame PDI. For cases of the SOI-40 and SOI-60, the overall flame PDI is decreased with the advancing of SOI timings. The lower

flame PDI essentially means a higher engine cycle-to-cycle variation and lower combustion stability. The variation of PDI at CA50 along a distance from the center of the bowl (a center line marked out in Fig. 7 for reference) is illustrated in Fig. 8. It shows that most of the flame region for the cases of SOI-30, SOI-40 and SOI-60 is located in the squish region and the flame region tends to move into the piston bowl with the advancing of the SOI timings. This trend is will be further discussed in section 3.2 combining the fuel distribution information.

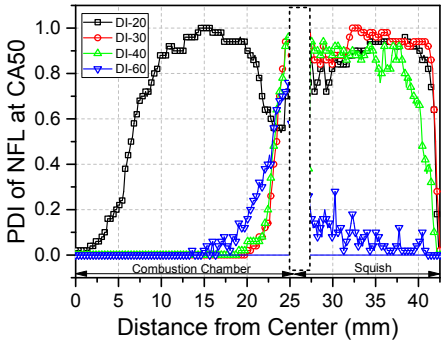

Fig. 8. The flame probability distribution index (PDI) along the center line at CA50 shown in Fig. 7a. The positions of the piston bowl and squish region are marked out. The piston bowl wall chamfer region is shown by a dashed black rectangle.

3.2 The spray-wall interaction under the different start of injection (SOI) timings

The averaged fuel-tracer PLIF images at different SOI timings are shown in Fig. 9. The overall fuel distribution in the piston bowl, squish region and piston top-land crevice can be visualized and linked to the flame PDI in Fig. 7. The single-shot images are presented in Fig. 10 to show the detailed local fuel spray characteristics. The false-color images later than -20° CA have the same scale of 0 to 5000 and other images have the scale from 0 to 7000. Note that the fuel injection duration is about 8° CA, so the first images of the SOI-20 case and SOI-60 case, as well as the first two images of the SOI-30 case and SOI-40 case, are during the fuel injection process.

For the SOI-20 case in Fig. 9a, the fuel spray first impinges on the piston bowl rim at -15° CA, and a large part of the fuel spray moves into the upper part of piston bowl and a small part into the squish region. When the fuel injection ends at -10° CA, the fuel in the upper bowl region goes into the lower part of the bowl while the fuel in the squish region penetrates deeper into the squish region, forming two relatively fuel-rich regions near the side wall of the bowl and piston top. When the heat release initiates at -5° CA, the fuel in the bowl occupies most of the bowl region and the fuel in the squish is very close to the cylinder wall but has not yet gone into the piston top-land crevice. Note that a higher PLIF intensity at the same crank angle (in-cylinder pressure and temperature) indicates a higher fuel-air equivalence ratio. Thus, the peak equivalence ratio in the squish regions is relatively higher than that in the piston bowl at -5° CA. This distribution can explain why the initial flame kernels first appear in the squish region at CA10 in Fig. 7. Subsequently, auto-ignition happens in the bowl region where most of the fuel resides in.

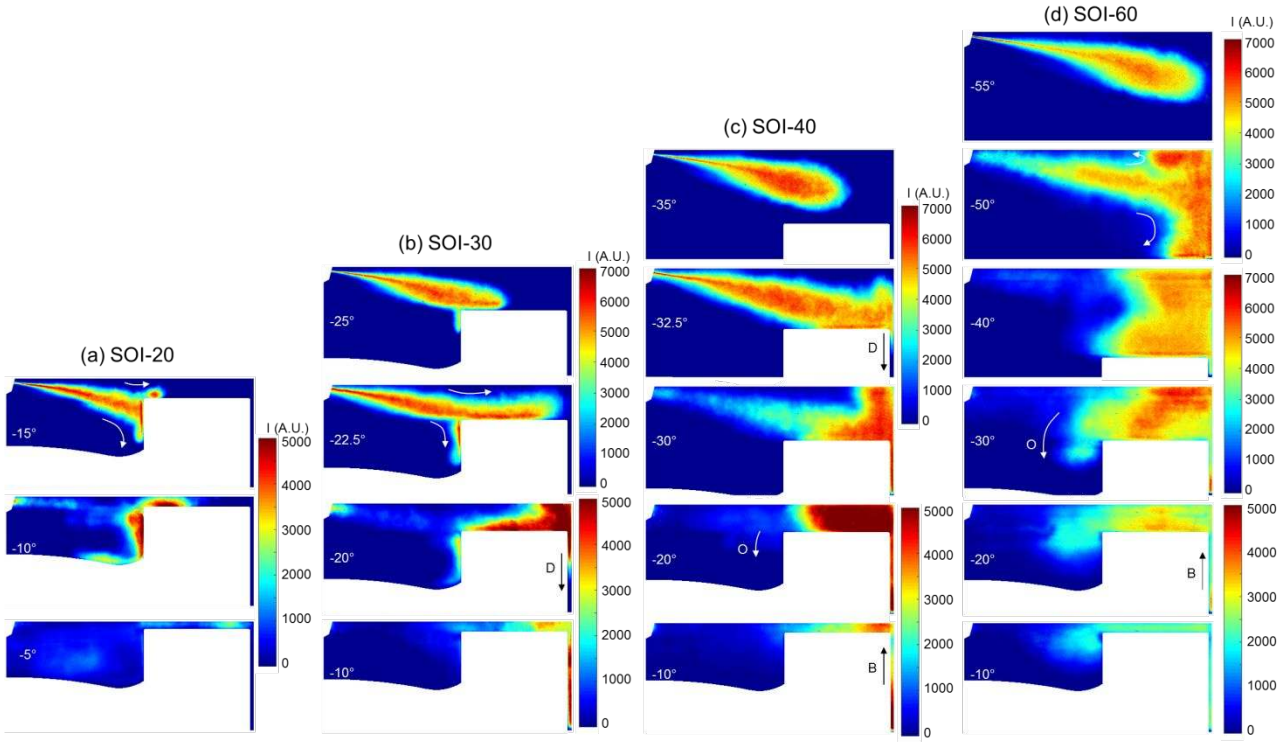

Fig. 9. The spray-wall interaction processes shown by the averaged PLIF images under different SOI timings: (a) SOI-20, (b) SOI-30, (c) SOI-40 and (d) SOI-60. The measurement crank angles (CA aTDC) are marked on the right of each averaged image. (D: downstream flow, B: backflow, O: overflow)

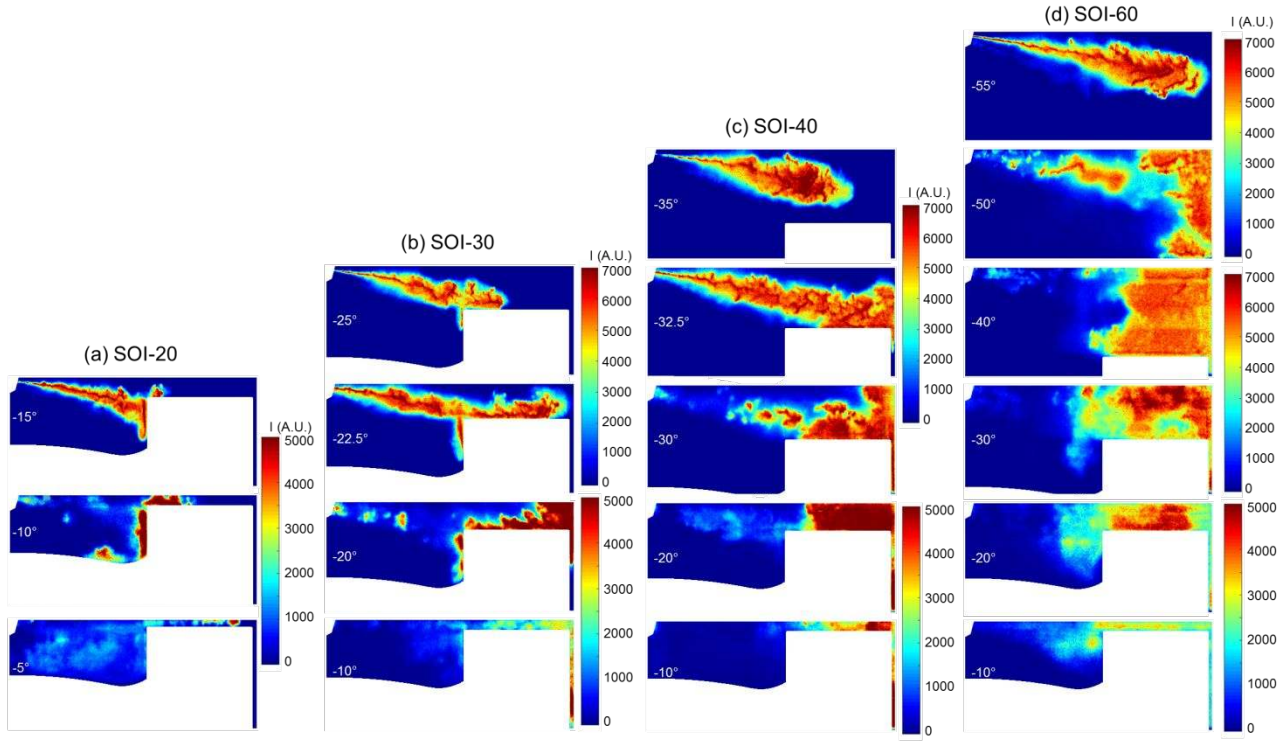

Fig. 10. The spray-wall interaction processes shown by the single-shot PLIF images under different SOI timings: (a) SOI-20, (b) SOI-30, (c) SOI-40 and (d) SOI-60. The measurement crank angles (CA aTDC) are marked on the right of each averaged image.

For the SOI-30 case in Fig. 9b, most of the fuel spray first touches the piston top at -25° CA and only a very small part of the spray spreads into the rim of the bowl. The fuel penetrates deeper into the squish region along the piston top surface at -22.5° CA, because the fuel injection has not ended at this time and the spray has very high momentum. It is very interesting to note that the single-shot PLIF images in Fig. 10 presents a clear view of the corrugated plumes inside the fuel spray. When the fuel injection ends at -20° CA, the spray head in the squish region hits on the cylinder wall, forming a relatively fuel-rich region wherein some part of fuel squeezes into the piston top-land crevice. The fuel in the crevice still has a certain momentum and thus it moves deeper downstream (shown by the white arrow "D") into the crevice. Most of the top-land crevice in the diagnostic region has been filled with the fuel-air mixture by -10° CA, which has a relatively higher equivalence ratio than that in the squish region, and very little fuel is distributed in the piston bowl region. The fuel distribution corresponds well with the flame PDI in Fig. 8 in which most of the flames are confined in the squish region for the SOI -30 case.

For SOI-40 case in Fig. 9c, the fuel spray has a longer penetration length at 5° CA after the start of injection (-35° CA aTDC) compared to the SOI-30 case due to lower in-cylinder pressure and temperature. The spray head just hits on the corner between the piston top and cylinder wall at -32.5° CA. The fuel with a higher momentum due to the lower in-cylinder pressure moves downstream into the top-land crevice with a faster speed. The top-land crevice in the view field has been completed distributed with the fuel-air charge at -30° CA when the fuel injection ends. When the piston moves up, the mixture in the squish region and top-land crevice is squeezed, and some part of the mixture in the squish region overflows into the piston bowl (shown by the white arrow "O"). At -10° CA, it is noteworthy to see a charge backflow process in the top-land crevice (shown by the black arrow "B") that results in a relatively lower equivalence ratio in the upper part of the crevice. Due to the backflow of the charge, the fuel distribution is also relatively richer in the squish region as against the SOI -30 case at the same crank angle.

As shown in Figure 9d, the SOI-60 case has the longest spray penetration length. The spray head almost touches the cylinder wall at 5° CA ASOI (-55° CA aTDC). The spray impinges on the cylinder wall without the interference of the piston top by the time of 10° CA ASOI (-50° CA aTDC), showing obvious two lateral vortexes as illustrated by the two white arrows. The spray momentum can be dissipated in these two vortexes, producing a wide fuel distribution area close to the cylinder wall. The fuel penetration into the piston top-land crevice impelled by the injection momentum, as shown in the SOI-30 and SOI-40 cases, cannot be seen here. When the piston moves up at -40° CA, the fuel-air charge in the squish region is compressed and the charge overflow into the piston bowl is more distinct at -30° CA. Meanwhile, the mixture closer to the cylinder wall stays and falls into the top-land crevice when the piston gradually approaches TDC. The backflow in the piston top-land crevice can be seen at -20° CA. Finally,

more fuel-air mixture diffuses into the bowl at -10° CA, resulting in a relatively lower equivalence ratio in the squish region and piston crevice compared to the other three cases at the same crank angle. This leads to the lower flame PDI in the squish region at CA50 but the flames are closer to the piston bowl center, as shown in Fig. 8.

In short, the spray-wall interaction locations move from the piston bowl wall to piston top and finally to the cylinder wall with the advancing of the SOI timings. A considerable portion of the fuel is trapped in the piston top-land crevice in cases of SOI-30 and SOI-40, forming relatively local fuel-rich regions there. The behavior of the fuel-air charge in the piston top-land crevice is different for the cases of SOI-30, SOI-40 and SOI-60. With much earlier SOI timing in the cases of SOI-40 and SOI-60, a backflow process from the crevice into the squish region can be seen after the fuel moving downstream into the top-land crevice. However, there is no time for the fuel-air charge to flow back before the start of combustion in the SOI-30 case, resulting in a relatively lower local fuel-air equivalence ratio in the squish region compared to that of the SOI-40 case. These different mechanisms of the fuel-air charge distribution in the top-land crevice could affect the engine combustion and emissions.

3.3 Discussion on the impact of the spray-wall interaction on the UHC and CO emissions of PPC at low load

As mentioned in the introduction section, Peterson et al. [22] found that most of the UHC and CO emissions came from the overly lean mixture ($0.1< \phi <0.5$) in the piston bowl and squish region. Subsequently, Ekoto et al. [30, 31] evaluated the UHC and CO emissions of PPC under the same optical engine with similar operating conditions. They reconstructed the late-cycle UHC and CO distribution in the upper part of the piston bowl and squish region combining PLIF imaging and multidimensional simulations. It showed that most of the UHC originated from the middle-upper part of the piston bowl close to the injector nozzle while the CO is mainly from the squish region at a load of about 3 bar IMEP, which is close to the engine load in the present study.

The UHC emission in Fig. 3 increases with the advancing of the SOI timings. It is easy to understand this trend based on Ekoto's finding because more overly lean mixture is generated in the main UHC formation region (middle-upper part of the piston bowl) due to a longer premixing time with earlier SOI timings. Normally, this trend also applies to the CO emission because the fuel-air equivalence ratio in the main CO formation region (squish region) should be decreased with the advancing of the SOI timings. However, Figure 3 presents a higher CO emission for the SOI-30 case compared to that of the SOI-40 case. In order to explain this anomalous phenomenon, we need to compare the fuel distributions in Fig. 9 for the SOI-30 case and SOI-40 case at -10° CA that is just before the initiation of the combustion. It shows that the overall fuel-air equivalence ratio in the squish region of the SOI-30 case is lower than that

of the SOI-40 case due to the fuel trapping effect of the piston top-land crevice. Thus, more overly lean mixture formed in the squish region could results in a higher CO emission for the SOI-30 case. This means that the fuel trapping effect of the piston top-land crevice has a great impact on the CO emission for the SOI-30 case, in which there is not enough time for the trapped fuel-air mixture to backflow into the squish region.

4. Conclusions

We studied the detailed spray-wall interaction under different SOI timings in an optical engine under PPC mode at low engine load. The distribution characteristics of the fuel trapped in the top-land crevice were visualized by the fuel-tracer PLIF imaging for the first time. The effects of the SOI timings on the combustion stability and engine-out emissions were analyzed. Some conclusions can be drawn as follows.

The gross IMEP and the NFL intensity at CA50 present a linear relationship under different SOI timings for PPC. The slopes of the linear fitting curves increase with the advancing of the SOI timings. The flame probability distribution index shows that the main combustion region first moves into the squish region and then tends to move back to the piston bowl with the advancing of the SOI timings. This trend is verified by the fuel distribution shown by the PLIF imaging.

The locations of the spray-wall interaction move from the piston bowl wall to piston top and finally to the cylinder wall with the advancing of the SOI timings. A considerable portion of the fuel is trapped in the piston top-land crevice for the SOI-30 case and SOI-40 case, forming relatively fuel-rich region there. The cases with much early SOI timings like SOI-40 and SOI-60 present a backflow process of the trapped fuel vapor from the top-land crevice to the squish region. However, there is not enough time for the fuel vapor to flow back before the start of combustion for the SOI-30 case, resulting in a relatively lower fuel-air equivalence ratio in the squish region than that of the SOI-40 case. This can account for the increase in the engine-out CO emission for the SOI-30 case compared to that of the SOI-40 case because studies in the literature showed that the CO emission mainly came from the overly lean mixture in the squish region at low engine load.

Acknowledgments

This work was funded by competitive research funding from King Abdullah University of Science and Technology (KAUST) and Saudi Aramco under the FUELCOM2 program. The authors would like to express our gratitude to our research Technicians, Riyadh Jambi and Adrian. I. Ichim for their support during the experiment at KAUST engine lab.

Appendix: image distortion correction

The image distortion from the side view comes from two parts: optical liner distortion and piston bowl distortion. The view fields in the squish region and piston bowl were corrected separately and then

put together. Take the optical liner distortion, for example, a target with a square grid was imaged by the ICCD camera with and without installing the liner. The grid images with and without distortion were used to produce a two-dimensional piecewise linear transformation matrix that can correct the distorted image, as shown in Fig. A1. We can see that the main image distortion is located in the squish region close to the liner wall on the right side from line 24 to 28.

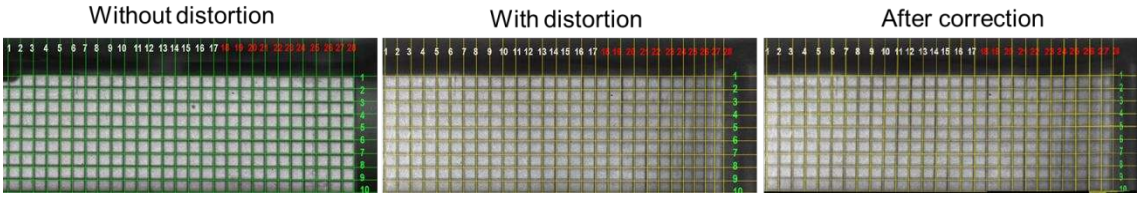

Fig. A1 Side view correction: optical liner distortion

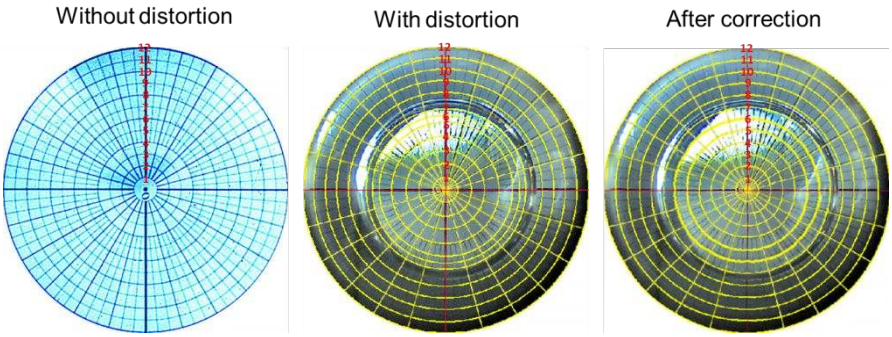

Fig. A2 Bottom view correction

Similarly, another transformation matrix derived from a polar coordinates target, as shown in Fig. A2 corrected the bottom view distortion produced by the piston. The main image distortion is in the region around the piston bowl from line 3 to 8 that has large curvature. Note that the corner between piston bowl wall and piston top has a small chamfer that results in excessive distortion. The signal in this region is unusable even after the mentioned correction, as shown in Fig. 7 and Fig. 8.

References

[1] Dec J. Advanced compression-ignition engines—understanding the in-cylinder processes. P Combust Inst. 2009;32(2):2727-42.

[2] Lu X, Ji L, Ma J, Zhou X, Huang Z. Combustion characteristics and influential factors of isooctane active-thermal atmosphere combustion assisted by two-stage reaction of n-heptane. Combust Flame. 2011;158(2):203-16.

[3] Liu P, Zhang Y, Wang L, Tian B, Guan B, Han D, et al. Chemical mechanism of exhaust gas recirculation on polycyclic aromatic hydrocarbons formation based on laser-induced fluorescence measurement. Energ Fuel. 2018;32(6):7112-24.

[4] Yao M, Zheng Z, Liu H. Progress and recent trends in homogeneous charge compression ignition (HCCI) engines. Prog Energ Combust. 2009;35(5):398-437.

[5] Benajes J, García A, Domenech V, Durrett R. An investigation of partially premixed compression ignition combustion using gasoline and spark assistance. Appl Therm Eng. 2013;52(2):468-77.

[6] Yao M, Zhang Q, Liu H, Zheng Z, Zhang P. Diesel engine combustion control: medium or heavy EGR? SAE 2010-01-1125. 2010.

[7] Noehre C, Andersson M, Johansson B, Hultqvist A. Characterization of partially premixed combustion. SAE 2006-01-3412. 2006.

[8] Miles PC, Collin R, Leif H, Hultqvist A, Andersson O. Combined measurements of flow structure, partially oxidized fuel, and soot in a high-speed, direct-injection diesel engine. P Combust Inst. 2007;31:2963-70.

[9] Kalghatigi GT, Risberg P, Angstrom H. Advantages of fuels with high resistance to auto-ignition in late-injection, low-temperature, compression Ignition Combustion. SAE 2006-04-3385. 2006.

[10] Kalghatgi GT, Risberg P, Ångström H. Partially pre-mixed auto-ignition of gasoline to attain low smoke and low NOx at high load in a compression ignition engine and comparison with a diesel fuel. SAE Paper 2007-01-0006. 2007.

[11] Manente V, Johansson B, Cannella W. Gasoline partially premixed combustion, the future of internal combustion engines? Int J Engine Res. 2011;12(3):194-208.

[12] Borgqvist P, Tunestal P, Johansson B. Comparison of negative valve overlap (NVO) and rebreathing valve strategies on a gasoline PPC engine at low load and idle operating conditions. SAE International Journal of Engines. 2013;6(1):366-78.

[13] Zhang X, Wang H, Zheng Z, Reitz RD, Yao M. Effects of late intake valve closing (LIVC) and rebreathing valve strategies on diesel engine performance and emissions at low loads. Appl Therm Eng. 2016;98:310-9.

[14] Hildingsson L, Kalghatgi G, Tait N, Johansson B, Harrison A. Fuel octane effects in the partially premixed combustion regime in compression ignition engines. SAE 2009-01-2648. 2009.

[15] Zheng Z, Yue L, Liu H, Zhu Y, Zhong X, Yao M. Effect of two-stage injection on combustion and emissions under high EGR rate on a diesel engine by fueling blends of diesel/gasoline, diesel/n-butanol, diesel/gasoline/n-butanol and pure diesel. Energy Conversion and Management. 2015;90:1-11.

[16] Vallinayagam R, An Y, S.Vedharaj, Sim J, Chang J, Johansson B. Naphtha vs. dieseline – The effect of fuel properties on combustion homogeneity in transition from CI combustion towards HCCI. Fuel. 2018;224:451-60.

[17] López JJ, García-Oliver JM, García A, Domenech V. Gasoline effects on spray characteristics, mixing and auto-ignition processes in a CI engine under Partially Premixed Combustion conditions. Appl Therm Eng. 2014;70(1):996-1006.

[18] Tang Q, Liu H, Li M, Yao M. Optical study of spray-wall impingement impact on early-injection gasoline partially premixed combustion at low engine load. Appl Energ. 2017;185:708-19.

[19] Fang T, Coverdill RE, Lee C-fF, White RA. Effects of injection angles on combustion processes using multiple injection strategies in an HSDI diesel engine. Fuel. 2008;87(15-16):3232-9.

[20] Li C, Yin L, Shamun S, Tuner M, Johansson B, Solsjo R, et al. Transition from HCCI to PPC: the sensitivity of combustion phasing to the intake temperature and the injection timing with and without EGR. SAE 2016-01-0767. 2016.

[21] Kook S, Park S, Bae C. Influence of early fuel injection timings on premixing and combustion in a diesel engine. Energ Fuel. 2008;22(1):331-7.

[22] Petersen B, Miles PC, Sahoo D. Equivalence ratio distributions in a light-duty diesel engine operating under partially premixed conditions. SAE International Journal of Engines. 2012;5(2):526-37.

[23] Wang Z, Lonn S, Matamis A, Andersson O, Tuner M, Alden M, et al. Transition from HCCI to PPC: investigation of fuel distribution by planar laser induced fluorescence (PLIF). SAE International Journal of Engines. 2017;10(4).

[24] Kim D, Ekoto I, Colban WF, Miles PC. In-cylinder CO and UHC imaging in a light-duty diesel engine during PPCI low-temperature combustion. SAE International Journal of Fuels and Lubricants. 2008;1(1):933-56.

[25] Kiplimo R, Tomita E, Kawahara N, Yokobe S. Effects of spray impingement, injection parameters, and EGR on the combustion and emission characteristics of a PCCI diesel engine. Appl Therm Eng. 2012;37:165-75.

[26] Koci CP, Ra Y, Krieger R, Andrie M, Foster DE, Siewert RM, et al. Detailed unburned hydrocarbon investigations in a highly-dilute diesel low temperature combustion regime. SAE 2009-01-0928. 2009.

[27] An Y, Vallinayagam R, Vedharaj S, Masurier J-B, Dawood A, Izadi Najafabadi M, et al. Analysis of transition from HCCI to CI via PPC with low octane gasoline fuels using optical diagnostics and soot particle analysis. SAE 2017-01-2403. 2017.

[28] Tang Q, Liu H, Li M, Yao M, Li Z. Study on ignition and flame development in gasoline partially premixed combustion using multiple optical diagnostics. Combust Flame. 2017;177:98-108.

[29] Hwang W, Dec J, Sjöberg M. Spectroscopic and chemical-kinetic analysis of the phases of HCCI autoignition and combustion for single- and two-stage ignition fuels. Combust Flame. 2008;154(3):387-409.

[30] Ekoto IW, Colban WF, Miles PC, Park SW, Foster DE, Reitz RD, et al. UHC and CO emissions sources from a light-duty diesel engine undergoing dilution-controlled low-temperature combustion. SAE 2009-24-0043. 2009.

[31] Musculus MPB, Miles PC, Pickett LM. Conceptual models for partially premixed low-temperature diesel combustion. Prog Energ Combust. 2013;39(2-3):246-83.